Temperature effect of nitrided stainless steel coatings deposited by reactive DC-magnetron sputtering

Terwagne, Guy; Colaux, Julie; Mitchell, D.; Short, K.

Published in:
Thin Solid Films

Publication date:
2004

Document Version
Publisher's PDF, also known as Version of record

Available online at www.sciencedirect.com
SCIENCE DIRECT
Thin Solid Films 469–470 (2004) 167–172
thin solid films
www.elsevier.com/locate/tsf

Temperature effect of nitrided stainless steel coatings deposited by reactive DC-magnetron sputtering

G. Terwagne[a,*], J. Colaux[a], D.R. Mitchell[b], K.T. Short[b]

[a]Laboratoire d'Analyses par Réactions Nucléaires, Facultés Universitaires Notre-Dame de la Paix, 61, rue de Bruxelles B-5000, Namur, Belgium
[b]Australian Nuclear Science and Technology Organisation, Lucas Heights PMB 1, Menai, Australia

Available online 5 November 2004

Abstract

Stainless steel coatings were deposited on low carbon steel and on monocrystalline silicon substrates by DC-magnetron sputtering in a reactive atmosphere containing argon and nitrogen. As the deposition process should be applied for industrial applications on in line and continuous processing, the substrates were grounded and not heated during the deposition. The nitrided stainless steel coatings were studied from the structural point of view. The preferential orientation (111) and/or (200) of the layers associated with the column-like morphology, underlined by X-ray diffraction (XRD) and transmission electron microscopy (TEM), is related to the thermal history of the coating growth. Interstitial nitrogen atoms are homogenously distributed in the *fcc* array of austenitic steel.

Keywords: Nitrided stainless steel coatings; DC-magnetron sputtering; Monocrystalline silicon substrate

1. Introduction

Whereas often employed for its excellent corrosion resistance, austenitic stainless steel is characterized by a poor hardness. An enhancement of wear resistance and reducing friction are both essential properties for many applications in metallurgy (machinery, tools,...) as well as in medicine (prosthesis, kneecap,...). In order to avoid these problems, a well-known technique is the nitriding of stainless steels. Nitrogen expanded austenite is obtained by different techniques, plasma-based [1–3] or implantation with nitrogen ion beams [4,5]. However, nitriding at temperature above 500 °C causes the precipitation of CrN [6] which removes Cr from solid solution affecting the corrosion performance of stainless steel. Reactive sputtering technique has the advantage that this process can be performed at room temperature allowing nitriding with very high nitrogen concentration without CrN precipitation. The purpose of this paper is to characterize the microstructure of coatings realized by reactive sputtering of AISI 304L stainless steel target in an Ar–N_2 atmosphere for different nitrogen flows. The temperature of the substrate is measured during deposition and will be related to the microstructure formed.

2. Experimental details

2.1. Sample preparation

Disks (diameter 20 mm) of low carbon steel with a thickness of 0.5 mm were mechanically polished with sandpapers of different grain sizes and finally to a mirror finish with diamond paste down to 1 μm. Silicon (100) wafers and steel samples were cleaned in an ultrasonic bath with pentane before loading in the chamber. The coatings were deposited using an unbalanced DC-magnetron sputtering system. A 50-mm diameter AISI-304L stainless steel (composition in wt.%: Fe 70%, Cr 18%, Ni 10%, Mn 2%) disk target was placed just above the magnets with a good thermal contact and was cooled with water during

* Corresponding author. Tel.: + 32 81 725478; fax: +32 81 725474.
E-mail address: guy.terwagne@fundp.ac.be (G. Terwagne).

0040-6090/$ - see front matter © 2004 Elsevier B.V. All rights reserved.
doi:10.1016/j.tsf.2004.08.101

deposition. A chimney was placed between the target and the sample holder placed 15 cm above the target to avoid contamination of the whole chamber. The magnetron power was set to 10 W cm^{-2}. The sample holder was heated by electrons and ions during deposition and the temperature of the specimen was measured using a thermocouple placed just behind. The coatings were reactively deposited onto monocrystalline (100) silicon (labeled Si) and on low carbon steel (labeled St) substrates for 10 to 60 min with various Ar/N_2 gas mixtures, which gave a thickness varying from 0.25 to 1.6 μm (Table 1). The proportion of N_2 in the sputter gas was varied by changing the N_2 flow rate with compensating adjustment of the Ar flow rate, such that the total gas flow rate remained constant at 35 SCCM. These flows correspond to a total pressure of 0.2–0.3 Pa measured with a baratron gauge placed in the deposition chamber.

2.2. Experimental techniques

The elemental characterization of the layers was performed at LARN (Namur, Belgium) by nuclear elemental analysis with ALTAÏS, the 2MV Tandetron accelerator [7]. The thickness and elemental composition (heavy elements) of the coatings were measured by Rutherford backscattering spectroscopy (RBS) and particle-induced X-ray emission (PIXE). Nuclear reaction analysis (NRA) was used to measure the nitrogen concentration using $^{14}N(d,p)^{15}N$ and $^{14}N(d,\alpha)^{12}C$ reactions with 1.1 MeV deuterons.

Transmission Electron Microscopy (TEM) conducted on a JEOL 2000FXII TEM operating at 200 keV and X-ray diffraction (XRD) were carried out at Ansto (Lucas Heights, Australia). Bragg–Brentano XRD patterns were obtained on a Siemens D500 diffractometer using Co Kα radiation (λ=1.789 Å) over Bragg angles from 2θ=30° to 2θ=130°, counting for 5 s at 0.05° intervals.

Table 1
Specifications of the coatings deposited on monocrystalline silicon or low carbon steel substrates

Sample	$t_{deposition}$ (min)	ΦN_2 (vol.%)	[N] (at.%)	Thickness (10^{15} at cm^{-2})	Thickness (μm)
St 1	40	0.0	0.30±0.03	12,000±1740	1.28±0.19
St 2	40	8.6	9.0±0.9	13,000±1885	1.39±0.20
St 3	60	14.3	13.5±1.3	16,500±2360	1.64±0.23
St 4	60	17.1	17.1±1.7	16,000±2288	1.56±0.22
St 5	60	22.9	16.5±1.7	16,000±2320	1.56±0.23
St 6	60	31.4	21.0±2.1	15,100±2190	1.41±0.20
St 7	60	37.1	24.0±2.4	13,400±1943	1.25±0.18
St 8	60	42.9	26.0±2.6	12,000±1716	1.12±0.16
Si 1	10	22.9	25.0±2.5	2600±520	0.25±0.05
Si 2	20	22.9	23.0±2.3	5100±765	0.49±0.07
Si 3	30	22.9	23.0±2.3	7700±1155	0.75±0.11
Si 4	40	22.9	22.0±2.2	10,000±1400	0.97±0.14
Si 5	50	22.9	22.0±2.2	12,600±1764	1.23±0.17
Si 6	60	22.9	22.0±2.2	15,600±2114	1.47±0.21

The nitrogen concentrations have been measured using $^{14}N(d,p)^{15}N$ and $^{14}N(d,\alpha)^{12}C$ nuclear reactions with 1.1 MeV deuterons and the thicknesses by RBS.

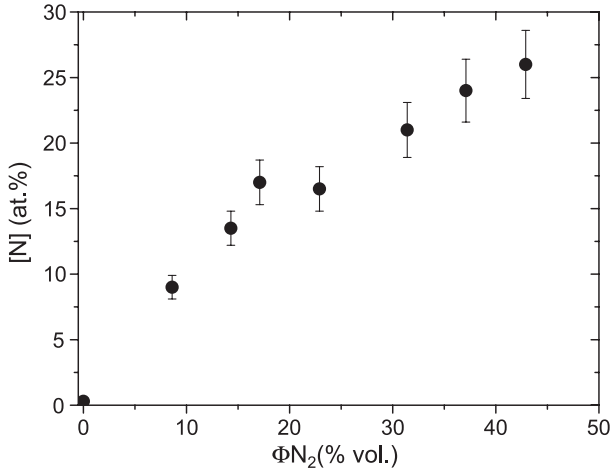

Fig. 1. The nitrogen concentration versus the nitrogen flow in the deposition chamber was measured for the nitrided stainless steel coatings deposited on low carbon steel. The linear increase corresponds to the metallic mode of deposition.

3. Results and discussion

Fig. 1 shows a proportional evolution of the nitrogen concentration measured by NRA versus the N_2 flow in the deposition chamber. We have observed previously that the nitrogen concentration is stable for higher nitrogen flows [7]. The linear increase of the N-concentration is related to the metallic mode of deposition. We have focused this study on this mode because the deposition rates are higher in this regime.

The structure of the coatings has been measured by XRD in the Bragg–Brentano geometry (Fig. 2a–i) and in grazing incidence (Fig. 2j–r). On the left figure, the peaks due to the substrate, shown in Fig. 2a, have been removed from the other data (Fig. 2c–i) in order to see the peaks due to the nitrided coatings. A background similar to the background shown in Fig. 2j has been subtracted on Fig. 2k to r in order to reveal the interesting patterns due to the nitrided coatings. The nitrogen concentration is indicated between the two figures. For both techniques, the patterns related to the coating performed without reactive gas correspond to a *bcc* structure (Fig. 2b and k). This result has already been observed by other authors [8]. A small amount of nitrogen is sufficient to stabilize the austenitic phase (Fig. 2c and l). The Bragg–Brentano geometry technique reveals two peaks corresponding to (111) and (200) orientations. The angular position of both peaks is decreasing when the N-concentration is increasing, which corresponds to an expansion of the austenite. The *d*-parameters versus nitrogen concentration are presented in Fig. 3. The *d*-parameter are increasing with the nitrogen concentration, which indicates that the expanded austenite is formed. This effect has also been observed by different authors [3,9–15]. A maximal intensity for the (111)

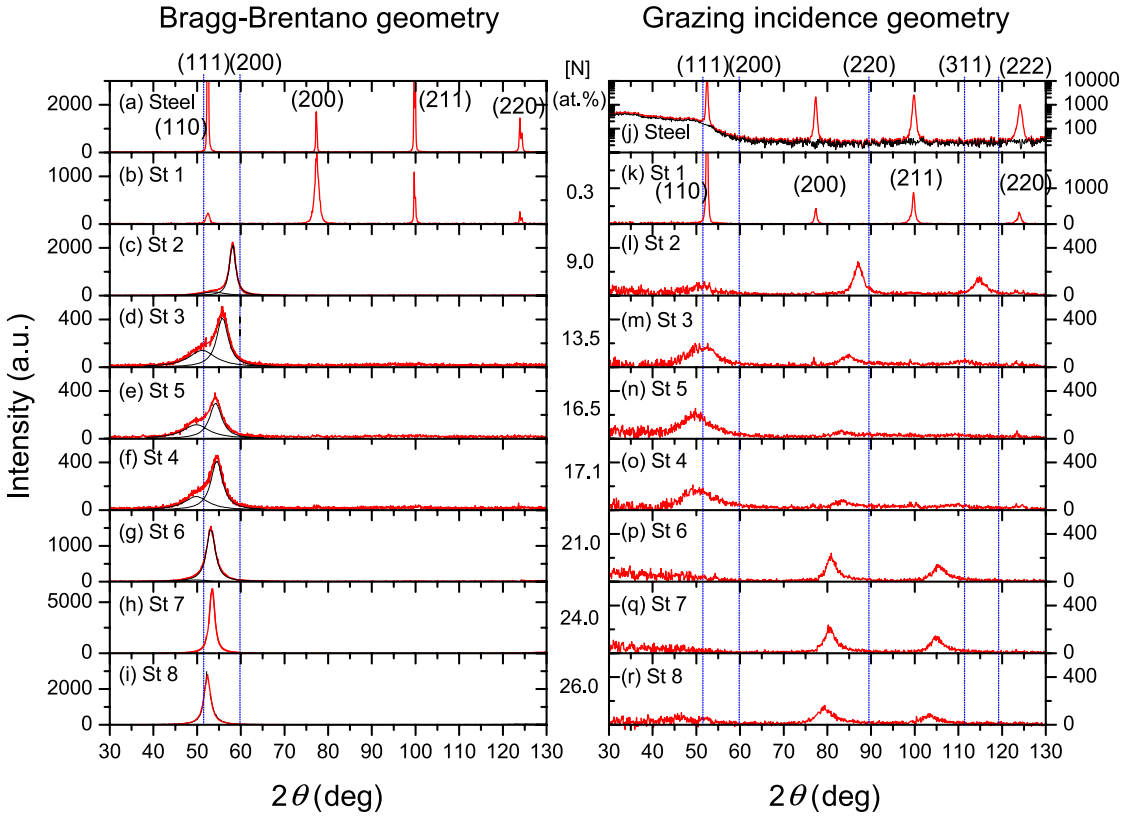

Fig. 2. On the left figure, the X-ray patterns are observed in the Bragg–Brentano geometry for the coatings deposited on low carbon steel substrate. The right figure shows the grazing incidence XRD pattern for the same specimens. The nitrogen concentration measured by $^{14}N(d,p)^{15}N$ and $^{14}N(d,\alpha)^{12}C$ is indicated between the two figures. The lines indicate the position of the planes corresponding to the *fcc* structures of stainless steel.

peak is observed when the nitrogen concentration reaches 13.5 at.%. The intensity of the (200) peak is higher than the (111) peak, which means that a preferential growing of the film along ⟨200⟩ axis occurs when the nitrogen concentration is increasing. This effect will be related to the temperature of the substrate. We observe also an expansion of austenite for the data recorded in grazing incidence XRD technique. The displacement of the (220) and the (222) peaks is increasing with the nitrogen concentration (Fig. 2l–r). Fig. 4 shows the evolution between the (220) and the (222) planes versus the N-concentration, which is nearly the same as the (111) plane (Fig. 3a). Preferential growing along ⟨200⟩ axis in the Bragg–Brentano geometry (Fig. 2c and g–i) is correlated with intense patterns for the (220) and (222) peaks in the GXRD geometry (Fig. 2l and p–r). For the intermediate N-concentrations (13.5 at.%≤[N]≤17.1 at.%), we observe a preferential orientation

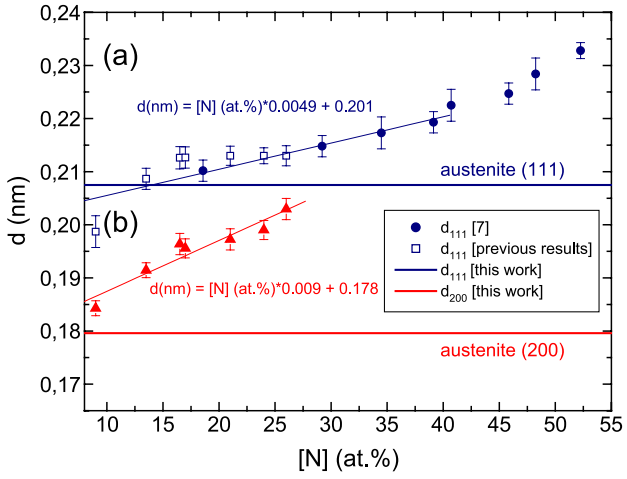

Fig. 3. The inter-planar spacing for the (200) and (111) planes measured by GXRD technique versus the nitrogen concentration is compared to previous results and to other results from the literature [7].

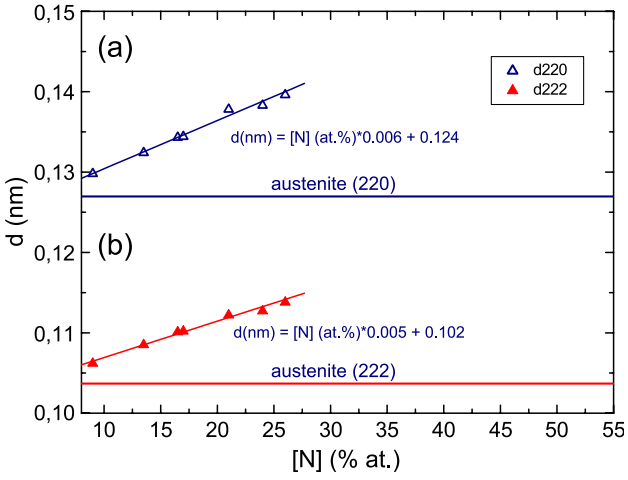

Fig. 4. The inter-planar spacing for the (220) and (222) planes measured by GXRD technique versus the nitrogen concentration is compared to previous results and to other results from the literature [7].

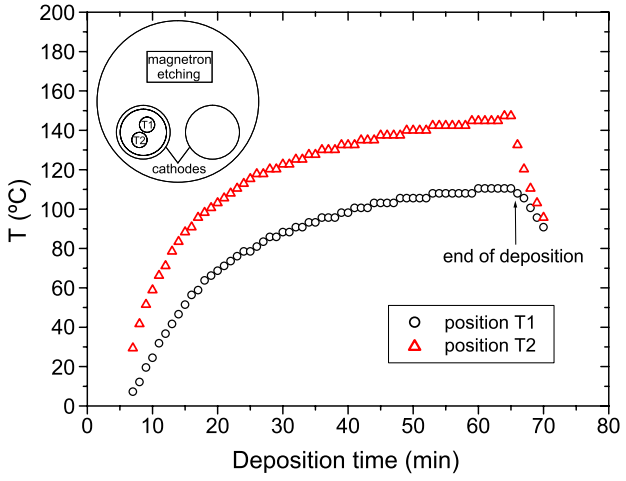

Fig. 5. Evolution of the substrate temperature measured during deposition onto silicon for two different places of the samples.

along the ⟨111⟩ axis. This effect is not related to the nitrogen concentration present in the coatings but to the temperature of the substrate during deposition.

In order to prove this temperature effect, we have performed two series of coatings on Si substrate (Samples Si 1 to Si 6 in Table 1) and measure the temperature during the deposition. The two sets of specimens were placed respectively in positions T1 and T2 (Fig. 5) and the temperature of both specimens was measured with two thermocouple (type K) placed at the rear of each sample. It is clearly seen in Fig. 5 that the evolution of the temperature depends on the position of the specimen in the chamber. This is principally due to the magnetron etching system located near the substrate holder and to the other cathode in the chamber. Our magnetron system is unbalanced [16] and the sample holder is not uniformly heated by the electrons ejected from the plasma. We can observe for both specimens placed in T1 and T2 that the temperature is increasing rapidly during 20 min and a saturation effect for longer deposition time. A systematic difference of 35 °C is also observed between both positions. We have measured both sets of samples (Si 1 to Si 6) using grazing incidence XRD technique and the results are presented in Fig. 6. We have also reported the sample temperature from the data plotted in Fig. 5. The (220) and (222) patterns appear when the temperature reach 90 °C for the samples in the T1 position (Fig. 6c) and when the temperature reaches 100 °C for the samples in the T2 position (Fig. 6h). The preferential growing along ⟨200⟩ axis, correlated to (220) and (222) patterns in the grazing incidence geometry, is possible for a substrate temperature upper than 100 °C. The reactivity of the substrate heated by the electrons ejected from the plasma is increased with the temperature and the preferential growing along ⟨200⟩ is observed.

TEM has been performed on the coatings deposited on monocrystalline silicon substrate as the sample preparation

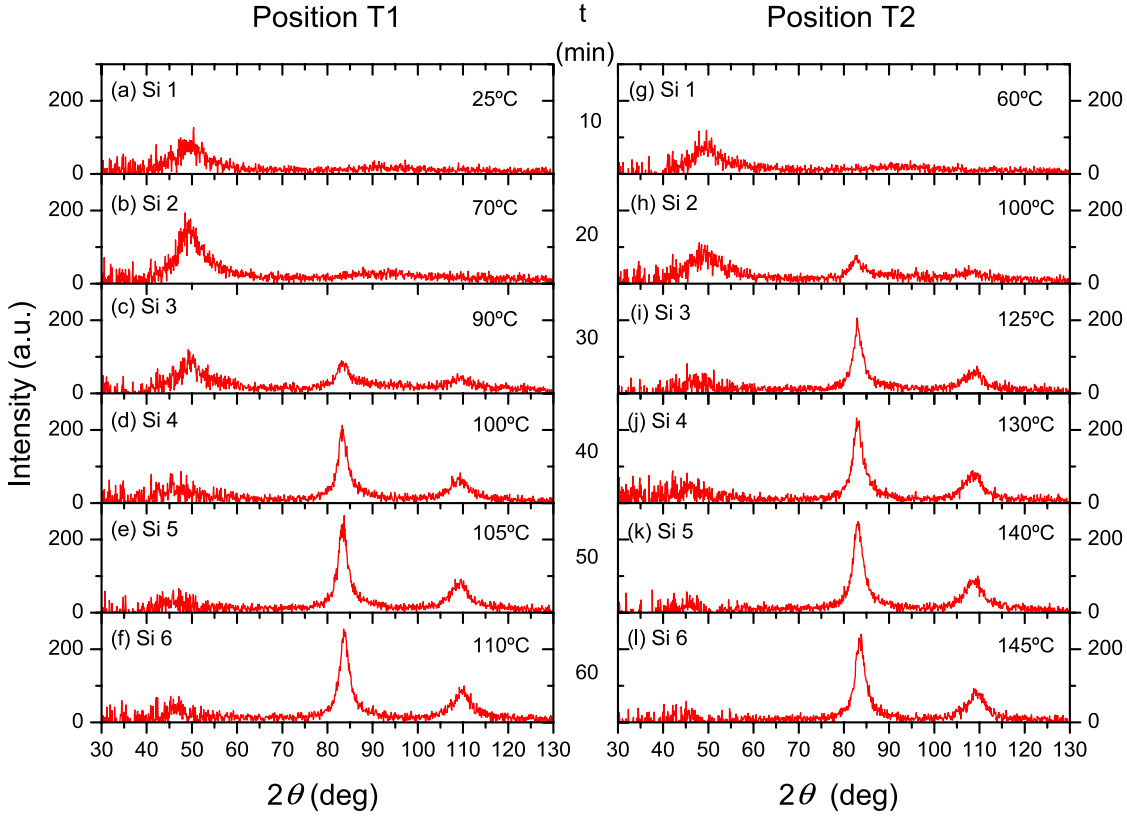

Fig. 6. GXRD patterns observed for coatings deposited on silicon substrates for different deposition time. The left and right figures correspond respectively to T1 and T2 positions. The final temperature is also indicated in each sub-figures.

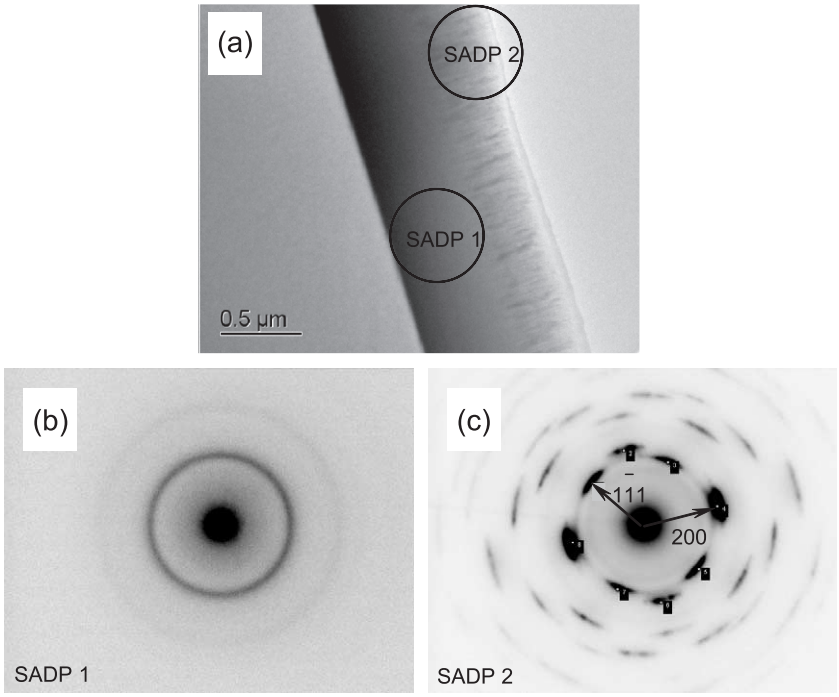

Fig. 7. Transmission electron micrograph of cross-section of specimen S5 (a). The selected area diffraction patterns of (b) and (c) were recorded in the SADP 1 and SADP 2, respectively.

is easier than for the low carbon steel substrate. Bright field image of a 1.25-μm nitrided coating deposited with 24% of nitrogen is shown in Fig. 7a. Diffraction patterns of electrons in the regions SADP 1 and SADP 2 are also presented in Fig. 7b and c. An amorphous structure is observed near the substrate while *fcc* and columnar structure are observed at the top of the layer. This effect is explained by the temperature during deposition. The first layers are deposited on the substrate at low temperature and an amorphous phase is observed while the top layers are deposited when the temperature is higher than 100 °C. A preferential growing of the coating along ⟨200⟩ axis with a columnar structure is than possible.

4. Conclusions

Morphology analyses show that during the early stages of deposition, the coating is amorphous for some tenth of microns. As the film gets thicker, the growth becomes columnar giving a fibrous texture. A correlation between amorphous thickness and nitrogen content does not seem evident. We suppose that this structure modification is caused by temperature history of the growing process. Indeed, substrate temperature has been monitored during deposition and it has been shown that this temperature increases between room temperature and more or less 140 °C. This effect is due to non-uniform electrons path coming from the unbalanced magnetron sputtering cathode. This path is deviated by other magnets near the sample holder. Electronic flow bombarding growing coating causes it to be heated non-uniformaly. When temperature reaches a sufficient value, the coating grows with fibrous texture. Regarding the substrate position in the deposition chamber, its final temperature evolves in a different way, the difference between positions being around 35 °C. Silicon substrates are not always at the same position from one time to another. That could explain why we do not see a linear dependence between nitrogen content and amorphous coating thickness. Bragg–Brentano X-ray diffraction made onto same samples has shown that when nitrogen concentration reaches 21 at.%, there is a (200) preferential growth. Indeed, (200) peak becomes very intense from this concentration. For nitrogen contents below 21 at.%, the (200) peak is seen by XRD but is not so intense. Electron diffraction has been made onto those samples and shows that the fibrous structure is *fcc* with (200) planes parallel to the silicon surface. So electron diffraction patterns are well correlated to XRD analysis.

Acknowledgments

We wish to thank Darren Attard of ANSTO for his expertise and training in the preparation of cross-sectional TEM specimens. This work was supported by the *Fonds de Recherche dans l'Industrie et l'Agriculture*.

References

[1] G.A. Collins, R. Hutchings, K.T. Short, J. Tendys, Surf. Coat. Technol. 103–104 (1998) 212.

[2] E. Menthe, K.T. Rie, J.W. Shultze, S. Simpson, Surf. Coat. Technol. 74–75 (1995) 412.
[3] K. Marchev, R. Hidalgo, M. Landis, R. Vallerio, C.V. Cooper, B.C. Giessen, Surf. Coat. Technol. 112 (1999) 67.
[4] F. Bodart, Th. Briglia, C. Quaeyhaegens, J. D'Haen, L.M. Stals, Surf. Coat. Technol. 65 (1994) 137.
[5] O. Orturk, D.L. Williamson, J. Appl. Phys. 77 (1995) 3839.
[6] Z.L. Zang, T. Bell, Surf. Eng. 1 (1985) 131.
[7] G. Terwagne, J. Colaux, G.A. Collins, F. Bodart, Thin Solid films 377–378 (2000) 441.
[8] B. Boubeker, J.P. Eymery, P. Auric, M. Rahmoune, Nucl. Instrum. Methods, B 101 (1995) 267.
[9] C. Blawert, B.L. Mordike, Y. Jiraskova, O. Scheeweiss, Surf. Coat. Technol. 116/119 (1999) 189.
[10] M. Samandi, B.A. Shedden, D.I. Smith, G.A. Collins, R. Hutchings, J. Tendys, Surf. Coat. Technol. 59 (1993) 261.
[11] D.L. Williamson, O. Orturk, S. Glich, R. Wei, P.J. Wilbur, Nucl. Instrum. Methods, B 59/60 (1991) 737.
[12] R. Leutenecker, G. Wagner, T. Louis, U. Gonser, L. Guzman, A. Molinari, Mater. Sci. Eng., A Struct. Mater.: Prop. Microstruct. Process. 115 (1989) 229.
[13] K. Ichii, K. Fujimuna, T. Takase, Technol. Rep. Kansai Univ. 27 (1986) 135.
[14] G.A. Collins, R. Hutchings, K.T. Short, J. Tendys, X. Li, M. Samandi, Surf. Coat. Technol. 74–75 (1995) 417.
[15] K.L. Dahm, P.A. Dearnley, Surf. Eng. 12 (1996) 61.
[16] M. Jacobs, G. Terwagne, PH. Roquiny, F. Bodart, Surf. Coat. Technol. 116–119 (1999) 735.